

CR-QAT: Curriculum Relational Quantization-Aware Training for Open-Vocabulary Object Detection

Jinyeong Park¹, Donghwa Kang², Brent ByungHoon Kang², Hyeongbooo Baek^{†3}, and Jibum Kim^{†1}

¹ Incheon National University, Incheon, South Korea

² KAIST, Daejeon, South Korea

³ University of Seoul, Seoul, South Korea

Corresponding authors: [†]hbbaek@uos.ac.kr, [†]jibumkim@inu.ac.kr

Abstract. Open-vocabulary object detection (OVOD) enables novel category detection via vision-language alignment, but massive model sizes hinder deployment on resource-constrained devices. While quantization offers practical compression, we reveal that naive extreme low-bit (*e.g.*, 4-bit) quantization severely degrades fine-grained vision-language alignment and distorts inter-region relational structures. To address this, we propose curriculum relational quantization-aware training (CR-QAT), an integrated framework combining stage-by-stage optimization with relational knowledge distillation. Within CR-QAT, curriculum QAT (CQAT) mitigates error accumulation by partitioning the model for progressive quantization, ensuring stable optimization via error isolation. Concurrently, text-centric relational KD (TRKD) is applied to task-relevant modules. By constructing text-anchored pairwise similarity matrices, TRKD comprehensively transfers the teacher’s multi-dimensional relational knowledge. Experiments on LVIS and COCO zero-shot benchmarks demonstrate that CR-QAT consistently outperforms existing QAT baselines under aggressive low-bit settings, achieving relative AP improvements of up to 38.9% and 40.9%, respectively.

Keywords: Open-vocabulary object detection · Quantization-aware training · Knowledge distillation

1 Introduction

The advent of vision-language models (VLMs) [21, 36] trained on large-scale image-text data has shifted the object detection paradigm toward open-vocabulary object detection (OVOD) [44], which leverages the transferred vision-language alignment [13, 24, 28, 46] to detect novel categories beyond predefined sets. However, relying on heavy ViT-based backbones and text encoders incurs massive computational overhead, hindering real-time edge deployment, and necessitating lightweight architectures.

To mitigate this, a recent paradigm exemplified by YOLO-World [7] decouples text and vision extraction by pre-computing text embeddings offline, thereby

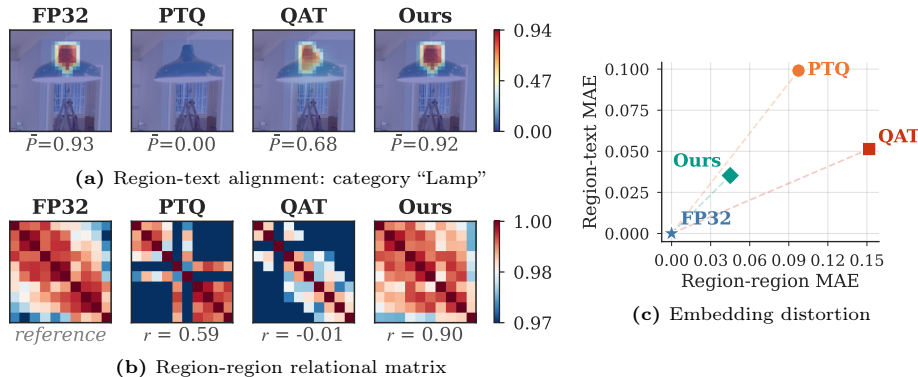


Fig. 1: Impact of 4-bit quantization on YOLO-World [7] with the Objects365v2 [40] dataset. (a) Confidence scores derived from the similarity between each region embedding and the text embedding of category “Lamp” (\bar{P} : mean over positive regions). (b) Pairwise cosine similarity matrix among positive region embeddings within the same category (r : Pearson correlation with FP32). (c) Quantitative comparison of embedding distortion relative to FP32. The horizontal and vertical axes measure the MAE of inter-region relational structure and region-text alignment, respectively. Proximity to the origin indicates less distortion. Our method simultaneously minimizes both, most closely approaching FP32.

eliminating the inference-time text encoder and enabling the use of a lightweight convolutional backbone [22]. Still, its ~ 180 MB model size remains a burden for embedded systems, requiring further compression such as pruning [16,17], knowledge distillation [5,18], or quantization [10,20].

Quantization is highly practical, replacing floating-point operations with efficient integer arithmetic without architectural changes. While quantization has achieved notable success in image classification [8,23,49,50], object detection poses greater challenges due to the dual need for fine-grained localization and classification [6]. Existing methods [6,15,25,43] address only closed-vocabulary settings, leaving a critical gap for OVOD models that depend heavily on precise vision-language alignment.

We investigate this gap by analyzing extremely low-bit (4-bit) quantization on YOLO-World with the Objects365v2 [40] dataset. Specifically, we examine how quantization affects the region-text alignment, which is the similarity between region and text embeddings. We also examine the inter-region relational structure, which captures pairwise similarities among region embeddings within the same text query. As shown in Fig. 1(a), post-training quantization (PTQ) destroys fine-grained region-text alignment, and naive QAT achieves only partial recovery. Furthermore, naive QAT fails to preserve semantic inter-region relationships (Fig. 1(b)). A quantitative comparison (Fig. 1(c)) further reveals that standard QAT fails to jointly minimize the mean absolute error (MAE) of both region-text alignment and inter-region relational structure. Under extreme capacity constraints, the model overfits to ground-truth matching scores, dis-

carding semantic inter-region relationships. These observations suggest that task loss alone cannot restore both fine-grained alignment and relational structure. Knowledge distillation (KD) is a natural candidate to address this limitation, as it is commonly used in QAT to transfer the full-precision teacher’s knowledge to the quantized student. However, in extreme low-bit settings, the substantial capacity gap between the teacher and the student introduces another challenge. Jointly optimizing task and KD losses becomes difficult, requiring a carefully designed distillation strategy [23].

To address these challenges, we propose a novel curriculum relational quantization-aware training (CR-QAT), an integrated framework that synergizes stage-by-stage optimization with module-wise knowledge distillation. Quantizing the entire network at once exacerbates error accumulation, as early-layer noise amplifies through subsequent modules [47]. To mitigate this, CR-QAT employs curriculum QAT (CQAT), partitioning the model into K functional units to progressively expand the quantization scope. Adapting CQAT to YOLO-World, we instantiate a two-stage curriculum: first quantizing the backbone while freezing the neck-head to isolate errors, followed by neck-head quantization for end-to-end sequential recovery. This establishes a stable optimization foundation.

To fully exploit this curriculum, CR-QAT incorporates text-centric relational KD (TRKD) alongside feature distillation, tailoring KD to each component’s functional role. We apply feature distillation to the task-agnostic backbone to recover representation capabilities. For the task-relevant neck-head, which handles cross-modal fusion and region-text matching, TRKD utilizes text embeddings as anchors to construct pairwise similarity matrices with assigned region embeddings. By constructing these matrices between teacher and student, TRKD comprehensively transfers multi-dimensional relational knowledge. Ultimately, CR-QAT successfully restores both fine-grained vision-language alignment and inter-region relational structures, simultaneously minimizing both embedding distortions to most closely approach the FP32 baseline (Fig. 1).

Our main contributions are summarized as follows:

- To the best of our knowledge, this is the first work to tackle extreme low-bit (*e.g.*, 4-bit) quantization for OVOD models. We systematically analyze the degradation of fine-grained vision-language alignment and inter-region relational structures.
- We propose CR-QAT, an integrated quantization learning framework. Within this, we introduce CQAT to mitigate error accumulation by partitioning the model for progressive, stage-by-stage quantization, ensuring stable optimization.
- We propose TRKD as a module-wise distillation strategy for task-relevant modules. TRKD constructs text-anchored pairwise similarity matrices to transfer the teacher’s multi-dimensional relational knowledge, simultaneously restoring distorted alignment and relational structures.
- Extensive experiments on LVIS and COCO zero-shot benchmarks demonstrate that CR-QAT consistently outperforms existing QAT baselines under

aggressive low-bit settings, achieving relative AP improvements of up to 38.9% and 40.9%, respectively.

2 Related Work

2.1 Open-Vocabulary Object Detection

Object detection has seen significant advancements through various paradigms, including two-stage [12, 39], one-stage [26, 29, 41], transformer-based [4, 45, 51], and YOLO-series [22, 37, 38, 42] architectures. However, these methods rely on a fixed set of training categories [27, 40]. This closed-vocabulary assumption prevents novel category detection, restricting their open-world applicability.

To overcome this, OVOD was introduced to detect novel categories via arbitrary text queries. Early work like OVR-CNN [44] established the standard OVOD setting, yet its generalization was limited by constrained vocabularies. With large-scale VLMs [21, 36], approaches began leveraging pretrained knowledge. ViLD [13], RegionCLIP [48], and OWL-ViT [31] transferred CLIP’s visual-semantic representations, while GLIP [24, 46] and Grounding DINO [28] reformulated object detection as region-text matching, achieving remarkable generalization. Nevertheless, most of these methods rely on heavy ViT backbones (*e.g.*, Swin-T [30]) and complex cross-modal fusion. This incurs massive computational complexity and memory footprints, hindering real-time deployment.

Recently, YOLO-World [7] introduced a “prompt-then-detect” paradigm using a lightweight YOLOv8 [22] architecture, enabling real-time OVOD by pre-computing text embeddings offline. Despite this progress, such lightweight models still retain a substantial number of parameters and intensive cross-modal operations, necessitating further compression for edge deployment. Quantization offers a practical solution by drastically reducing computational costs without architectural modifications. Therefore, designing an effective quantization technique that preserves the fine-grained vision-language alignment of OVOD models is a critical challenge.

2.2 Quantization for Object Detection

Network quantization reduces memory and computational overhead by representing models in low-bit precision. Broadly categorized into PTQ [9, 32, 33] and QAT [2, 8, 10, 20, 49], it has achieved notable success in image classification. While object detection quantization has been explored, it remains less investigated. Early methods [20, 25, 52] were limited to 8-bit precision, struggled with training instability, or imposed architectural constraints. To achieve accurate, fully quantized object detection, subsequent works proposed multi-level batch normalization [6], weight oscillation mitigation [15, 34], and distribution rectification distillation for transformer-based detectors [43].

Since standard QAT struggles to fully recover performance in extreme low-bit settings, integrating knowledge distillation (KD) has become a prevalent

approach. In image classification, distilling outputs or intermediate features from a full-precision teacher effectively enhances the quantized student’s performance [23, 35, 50]. Similarly, task-specific KD designs have proven highly effective in dense prediction tasks like object detection [43] and BEV-based 3D detection [47].

However, all aforementioned studies are strictly confined to closed-vocabulary settings. The quantization of OVOD models, which heavily rely on fine-grained vision-language alignment, remains an unexplored territory. To bridge this gap, our work proposes CR-QAT, an effective low-bit quantization learning framework tailored specifically for OVOD models.

3 Preliminaries

In this section, we briefly review the fundamental concepts of network quantization and open-vocabulary object detection, which form the basis of our proposed framework.

3.1 Quantization

We assume uniform quantization for weights and activations. For a parameter $w \in \mathbb{R}$, b -bit uniform quantization maps it to a discrete level. Given a scale $s > 0$, a zero-point $z \in \mathbb{Z}$, and a range $[l, u]$ defined by the bit-width b , the process is defined as:

$$\bar{w} = \left\lfloor \text{clip}\left(\frac{w}{s} + z, l, u\right) \right\rfloor, \quad (1)$$

where $\lfloor \cdot \rfloor$ denotes round-to-nearest, and $\text{clip}(x, l, u)$ bounds the value within $[l, u]$. The range is $[-2^{b-1}, 2^{b-1} - 1]$ for signed and $[0, 2^b - 1]$ for unsigned integers. The dequantized parameter \hat{w} is reconstructed as:

$$\hat{w} = (\bar{w} - z) \cdot s. \quad (2)$$

This scheme is termed symmetric quantization when $z = 0$, and asymmetric otherwise.

Quantization-aware training (QAT) simulates these operations during training. In the forward pass, w undergoes quantize-dequantize steps (Eqs. (1) and (2)) to compute the loss \mathcal{L} . During backpropagation, the straight-through estimator (STE) [1] approximates gradients through the non-differentiable rounding operator. Furthermore, s and z can be jointly optimized as learnable parameters [2, 10], allowing the model to actively compensate for quantization errors and yielding significant gains over post-training quantization in low-bit settings.

3.2 Open-Vocabulary Object Detection

Closed-vocabulary detectors [4, 29, 37, 39] rely on a parameterized classifier tailored to a fixed set of training categories $\mathcal{C}_{\text{base}}$. Consequently, they cannot detect novel categories in open-world scenarios. Open-vocabulary object detection (OVOD) [7, 24, 44] transcends this by detecting unseen categories $\mathcal{C}_{\text{novel}}$

($\mathcal{C}_{\text{base}} \cap \mathcal{C}_{\text{novel}} = \emptyset$) during inference, despite training solely on $\mathcal{C}_{\text{base}}$ annotations [44].

This is prominently achieved by replacing the fixed classifier with text embeddings. OVID models [7, 24, 46] utilize dual encoders: an image encoder for multi-scale visual features and a text encoder for arbitrary category queries. These features interact through fusion modules (*e.g.*, cross-attention) to establish fine-grained vision-language alignment.

A region embedding $\mathbf{v} \in \mathbb{R}^D$ is then extracted for each candidate region. Final classification relies on the cosine similarity between \mathbf{v} and the text embedding $\mathbf{t} \in \mathbb{R}^D$:

$$s = \text{sim}(\mathbf{v}, \mathbf{t}). \quad (3)$$

Leveraging text encoders pretrained on massive datasets [36], this region-text matching seamlessly extends detection to both $\mathcal{C}_{\text{base}}$ and $\mathcal{C}_{\text{novel}}$ simply by altering the query set.

Given an input image x and ground-truth annotations $y = \{(b_i, c_i)\}_{i=1}^{N_{\text{gt}}}$ for base categories $c_i \in \mathcal{C}_{\text{base}}$ and bounding boxes b_i , the model optimizes:

$$\mathcal{L}_{\text{task}}(x, y) = \mathcal{L}_{\text{cls}}(x, y) + \mathcal{L}_{\text{loc}}(x, y), \quad (4)$$

where \mathcal{L}_{cls} and \mathcal{L}_{loc} denote the region-text similarity-based classification loss and bounding box regression loss, respectively.

Crucially, this detection capability relies entirely on the fine-grained alignment between region and text embeddings. If extreme low-bit quantization distorts this embedding space, it catastrophically degrades both the fine-grained vision-language alignment and inter-region relational structures, severely impairing classification performance. Resolving these multi-dimensional distortions is the primary motivation behind our proposed CR-QAT framework.

4 Method

CR-QAT is an integrated framework that mitigates quantization error accumulation and comprehensively restores multi-dimensional relational knowledge. It consists of two synergistic components: CQAT for stable, stage-by-stage optimization, and TRKD tailored for task-relevant modules to reconstruct fine-grained vision-language alignments and inter-region relational structures.

4.1 Curriculum QAT

Standard QAT quantizes all layers simultaneously to optimize the task loss $\mathcal{L}_{\text{task}}$. However, in extreme low-bit settings, quantization errors originating from early modules accumulate rapidly and propagate through subsequent layers. This results in severe degradation of representation capability, making recovery extremely difficult [47].

To overcome this, CQAT partitions the model into K functional units $\{M_1, M_2, \dots, M_K\}$ and progressively expands the quantization scope along the data

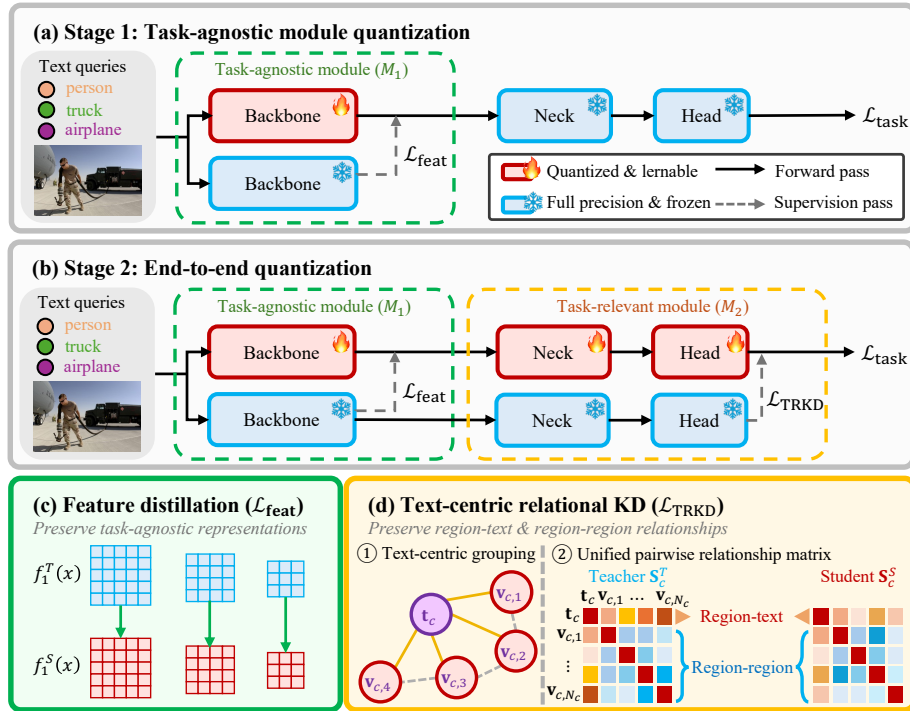


Fig. 2: Overview of the proposed CR-QAT framework. (Red) blocks denote quantized and learnable modules, and (blue) blocks denote full-precision and frozen modules. (a) Stage 1: the backbone (M_1) is quantized with \mathcal{L}_{feat} supervision from the full-precision teacher, while the neck-head remains frozen for error isolation. (b) Stage 2: the neck-head (M_2) is additionally quantized, supervised by both \mathcal{L}_{feat} and \mathcal{L}_{TRKD} . (c) Feature distillation aligns the student’s multi-scale backbone features $f_1^S(x)$ to those of the teacher $f_1^T(x)$. (d) TRKD groups region embeddings by text query t_c and constructs a unified pairwise similarity matrix S_c to transfer region-text and region-region relationships.

flow. Let \mathbf{w}_k be the weights and ϕ_k be the quantization parameters (e.g., scaling factor, zero-point) of module M_k . At stage k , we apply quantization strictly to the first k modules while freezing the remaining modules (M_{k+1}, \dots, M_K) in full-precision. The objective at stage k is formulated as:

$$\arg \min_{\{\mathbf{w}_i, \phi_i\}_{i=1}^k} \mathcal{L}_{task}(x, y \mid \{\mathbf{w}_i, \phi_i\}_{i=1}^k, \{M_j^{FP}\}_{j=k+1}^K). \quad (5)$$

The core principles underlying this design are *error isolation* and *sequential recovery*. Error isolation prevents premature noise propagation; unquantized modules retain the capacity to process degraded intermediate features and provide stable backward gradients. Sequential recovery ensures that when module M_k is newly quantized, it receives higher-quality inputs from preceding optimized modules, allowing it to focus on compensating for its own quantization error.

For widely-adopted OVOD architectures (*e.g.*, GLIP [24], YOLO-World [7]), we instantiate a two-stage curriculum ($K = 2$). As illustrated in Fig. 2, Stage 1 (Fig. 2(a)) quantizes the task-agnostic backbone (M_1) to recover multi-scale feature degradation, utilizing the frozen neck-head (M_2) as an error isolator. Stage 2 (Fig. 2(b)) subsequently quantizes the neck-head to complete end-to-end optimization. We integrate the neck and head into a single module, as both are task-relevant components that jointly handle cross-modal fusion and region-text matching. Furthermore, separating them would require an independent KD strategy for the neck, yet distilling its multi-scale feature pyramids is known to be unstable under low-bit constraints [50]. Grouping them avoids this issue and reduces the complexity of the training pipeline (see Sec. 5).

4.2 Text-Centric Relational KD

While CQAT structurally mitigates error accumulation, the information lost due to severe bit-width reduction remains substantial. To enhance sequential recovery, CR-QAT integrates module-wise KD into each curriculum stage. By leveraging the stable optimization foundation of CQAT, KD becomes effective even under restricted low-bit capacities. We tailor the KD strategy to the functional role of each module. Given a full-precision teacher, the total loss at stage k is:

$$\mathcal{L}_{\text{stage } k} = \mathcal{L}_{\text{task}} + \sum_{i=1}^k \lambda_i \mathcal{L}_{\text{KD}}^{(i)}, \quad (6)$$

where $\mathcal{L}_{\text{KD}}^{(i)}$ is the KD loss specifically designed for module M_i , and λ_i is its balancing weight. As the curriculum progresses, KD losses from previous stages are retained as regularizers to prevent re-degradation.

Backbone (M_1): Feature Mimicking. As a task-agnostic feature extractor, the backbone’s output quality fundamentally dictates the performance of all subsequent modules. Thus, we directly mimic the multi-scale features of the teacher’s backbone (Fig. 2(c)) using PKD [3]:

$$\mathcal{L}_{\text{KD}}^{(1)} = \mathcal{L}_{\text{feat}}(f_1^S(x), f_1^T(x)), \quad (7)$$

where $f_1^S(x)$ and $f_1^T(x)$ denote the backbone output features of the student and teacher, respectively.

Neck-head (M_2): TRKD. The task-relevant neck-head governs the fine-grained vision-language alignment. Extreme low-bit quantization severely distorts both region-text alignment and inter-region relational structures, which standard distillation cannot adequately restore. To address this, we propose TRKD, which uses text embeddings as anchors to capture both relationships within a unified pairwise similarity matrix (Fig. 2(d)).

For each text query c , TRKD constructs a matrix comprising its text embedding \mathbf{t}_c and N_c assigned region embeddings $\{\mathbf{v}_{c,n}\}_{n=1}^{N_c}$:

$$\mathbf{X}_c = [\mathbf{t}_c \ \mathbf{v}_{c,1} \ \cdots \ \mathbf{v}_{c,N_c}]^\top \in \mathbb{R}^{(1+N_c) \times D}, \quad (8)$$

where D is the embedding dimension. The specific region assignment strategy depends on the base architecture (Sec. 5). After row-wise L2-normalization to obtain $\hat{\mathbf{X}}_c$, we compute the pairwise cosine similarity matrix:

$$\mathbf{S}_c = \hat{\mathbf{X}}_c \hat{\mathbf{X}}_c^\top \in \mathbb{R}^{(1+N_c) \times (1+N_c)}. \quad (9)$$

The first row and column of this matrix explicitly encode the region-text alignments, while the remaining internal blocks capture the region-region relationships. We compute this matrix for both the teacher and the student, denoted \mathbf{S}_c^T and \mathbf{S}_c^S , respectively. By minimizing their discrepancy, the student retains the teacher’s multi-dimensional relational structure:

$$\mathcal{L}_{\text{KD}}^{(2)} = \frac{1}{|\mathcal{C}|} \sum_{c \in \mathcal{C}} \frac{1}{(1+N_c)^2} \sum_{i=1}^{1+N_c} \sum_{j=1}^{1+N_c} \ell_\delta(S_{c,ij}^S, S_{c,ij}^T), \quad (10)$$

where \mathcal{C} is the set of text queries in the image, and ℓ_δ denotes the Smooth L1 loss. By applying an element-wise average per text and subsequently averaging across all texts, we ensure that relational structures with fewer assigned regions are equally represented in the optimization process.

5 Experiments

We evaluate CR-QAT on YOLO-World under extreme low-bit (4-4-8) quantization settings across LVIS and COCO zero-shot benchmarks, and conduct comprehensive ablation studies to validate each component.

5.1 Experimental Settings

Datasets and Evaluation. For QAT training, we use the Objects365v2 [40] train split and GQA [19]. Following YOLO-World [7], zero-shot evaluation is conducted on LVIS `minival` with the Fixed AP protocol [14] and COCO [27] `val2017`.

Quantization Settings. We use official pre-trained YOLO-World-M/L/X checkpoints. The text encoder (CLIP [36]) is excluded from quantization, as it is removed at inference by pre-computing text embeddings offline [7]. We apply symmetric quantization for weights and asymmetric for activations and attentions. Our main results adopt a 4-4-8 bit-width configuration (weight-activation-attention) with Ch-T-H granularity (per-channel weight, per-tensor activation, per-head attention). The first and last layers remain unquantized, following common practice [8, 49]. For calibration, we use 256 samples from the Objects365v2 validation set.

Table 1: LVIS miniVal zero-shot evaluation with 4-4-8 quantization (Ch-T-H granularity). Ch = per-channel, T = per-tensor, H = per-head. Evaluation follows the LVIS fixed AP protocol [14].

Model	Bits	Size(MB)	BOPs(T)	Method	AP	AP _r	AP _c	AP _f
YOLO-World-M	FP32	110.88	51.82	-	28.6	19.7	26.6	31.9
	4-4-8	15.11	7.10	QAT Ours	12.3 14.8 (+20.3%)	8.2 9.2	10.2 13.0	14.9 17.5
YOLO-World-L	FP32	181.4	98.39	-	32.9	23.6	31.9	35.5
	4-4-8	24.32	8.18	QAT Ours	11.4 14.8 (+29.8%)	6.1 11.8	9.8 13.2	13.7 16.8
YOLO-World-X	FP32	281.11	149.08	-	33.4	24.4	31.5	36.6
	4-4-8	37.19	9.32	QAT Ours	10.8 15.0 (+38.9%)	4.1 9.3	9.5 12.9	13.1 17.9

Training Details. We adopt the YOLO-World pretraining configuration, except for the learning rate of 1.5×10^{-5} and the batch size of 48 for QAT. The learning rate scheduler is disabled as we fine-tune for 1 epoch. The text encoder remains frozen. Quantization parameters are learned via LSQ [2, 10] with a learning rate of $0.1 \times$ the base rate. Curriculum stage 1 (backbone) uses the first 1/3 of the data, while stage 2 (neck-head) uses the remaining 2/3. The KD loss weight λ_i is 6.0 for both feature distillation and TRKD. For TRKD, regions assigned to each text query are positive samples determined by the teacher’s task-aligned label assignment (TAL) [11].

5.2 Main Results

The 4-4-8 (W4A4) with per-tensor activation quantization is a highly aggressive setting. PTQ suffers severe performance collapse (AP 0.0) across all models on both LVIS and COCO regardless of calibration strategy (MinMax, Percentile [25], OMSE [9]), demonstrating that low-bit quantization of OVOD models is infeasible without training. The QAT baseline simultaneously quantizes all layers and trains with only the task loss $\mathcal{L}_{\text{task}}$, using LSQ [2, 10], a widely adopted learnable quantization scheme. For fair comparison, the baseline shares the same training configuration, total data, and number of iterations as CR-QAT. Under this setting, 4-4-8 quantization reduces model size by up to $7.6 \times$ and bit operations (BOPs) by up to $33.4 \times$ (reported per benchmark in Tabs. 1 and 2, as BOPs vary with the number of text queries). In Sec. 5.4, we further show that CR-QAT consistently outperforms QAT even under finer granularity settings where absolute performance is substantially higher.

LVIS MiniVal Zero-Shot. LVIS [14] contains 1,203 object categories, each classified by annotation frequency into rare (AP_r), common (AP_c), and frequent

Table 2: COCO Val2017 zero-shot evaluation with 4-4-8 quantization (Ch-T-H granularity)

Model	Bits	BOPs(T)	Method	AP	AP ₅₀	AP ₇₅	AP _s	AP _m	AP _l
YOLO-World-M	FP32	44.56	-	41.9	57.0	45.5	26.7	46.1	55.0
	4-4-8	2.05	QAT	22.0	32.1	23.6	7.8	23.5	32.4
			Ours	25.1 (+18.6%)	38.1	28.1	11.0	28.1	37.9
YOLO-World-L	FP32	90.60	-	45.1	60.7	48.9	29.8	49.8	57.5
	4-4-8	3.09	QAT	18.4	27.2	19.6	7.5	20.1	26.9
			Ours	25.2 (+37.0%)	36.7	27.0	10.5	27.5	37.7
YOLO-World-X	FP32	140.66	-	46.7	62.8	50.9	31.8	51.2	60.8
	4-4-8	4.21	QAT	18.6	26.8	19.9	7.8	20.5	27.0
			Ours	26.2 (+40.9%)	38.2	28.1	12.2	28.7	37.2

(AP_f). The large number of categories and the high proportion of rare categories make it a benchmark that directly reflects the difficulty of open-vocabulary detection. Table 1 reports results for YOLO-World-M/L/X. While QAT recovers from the complete failure of PTQ, a large gap relative to FP32 remains, with drops of -16.3 AP on YOLO-World-M and -21.5 on YOLO-World-L. CR-QAT consistently outperforms QAT across all models, with improvements of $+2.5$, $+3.4$, and $+4.2$ AP on YOLO-World-M, L, and X, respectively. Notably, QAT degradation grows with model scale, yet our improvement trend follows the same direction, indicating that our method becomes more beneficial as the capacity gap widens. The gains are particularly pronounced in AP_r, which measures rare category detection and serves as a key indicator of open-vocabulary capability [7, 24]. Since rare categories heavily depend on vision-language alignment quality, the substantial AP_r gains of $+5.7$ on YOLO-World-L and $+5.2$ on YOLO-World-X, corresponding to 93.4% and 126.8% relative improvements, demonstrate that CR-QAT effectively restores the fine-grained alignment damaged by quantization.

COCO Val2017 Zero-Shot. COCO [27] contains 80 categories with scale-wise evaluation across small (AP_s), medium (AP_m), and large (AP_l), making it suitable for assessing scale robustness. As shown in Tab. 2, PTQ again completely fails with AP 0.0, and QAT leaves a large gap from FP32. CR-QAT consistently outperforms QAT, with improvements of $+4.1$ and $+6.8$ AP on YOLO-World-M and YOLO-World-L, and the gain further increases to $+7.6$ AP (40.9%) on YOLO-World-X, again confirming larger gains at greater model scales. These improvements also hold across all object scales, as illustrated by YOLO-World-M where AP_s, AP_m, and AP_l improve by $+3.2$, $+4.6$, and $+5.5$, respectively. The $+7.4$ gain in AP₇₅ on YOLO-World-L further demonstrates effective recovery of

Table 3: Ablation on CR-QAT components. KD includes feature distillation and TRKD. LVIS miniVal AP is reported.

Curriculum	KD	AP
✗	✗	11.4
✓	✗	12.6
✗	✓	11.8
✓	✓	14.8

Table 4: TRKD component analysis. All variants use CQAT with feature distillation. LVIS miniVal AP is reported.

TRKD variant	AP
w/o TRKD (feat only)	13.1
region-text	13.7
region-region	14.3
full TRKD	14.8

localization precision, confirming that CR-QAT restores not only classification alignment but also fine-grained localization capability.

5.3 Ablation Studies

Ablations on CR-QAT. Table 3 analyzes the individual contributions of the curriculum strategy and KD on YOLO-World-L with 4-4-8 (Ch-T-H) quantization. Applying only the curriculum (CQAT) to QAT (AP 11.4) yields AP 12.6 (+1.2), while applying KD alone yields only AP 11.8 (+0.4). This indicates that KD struggles without the stable optimization foundation provided by the curriculum. Combining both achieves AP 14.8 (+3.4), far exceeding the sum of their individual gains (+1.6). This strong synergy confirms that the curriculum is an essential foundation for KD to operate effectively.

Ablations on TRKD. Table 4 decomposes TRKD into its two components: region-text alignment and region-region relationships. Using only CQAT with backbone feature distillation (*i.e.*, without TRKD) yields AP 13.1, which serves as the baseline. Distilling only region-text alignment yields AP 13.7 (+0.6), while region-region only achieves AP 14.3 (+1.2). Both components contribute meaningfully, and full TRKD achieves the best AP of 14.8 by preserving both simultaneously. This confirms that region-text alignment and inter-region relational structure are complementary for restoring the teacher’s multi-dimensional relational knowledge.

Effect of Curriculum Stages. Table 5 compares two-stage (backbone→neck-head) and three-stage (backbone→neck→head) curriculum strategies. Three-stage consistently underperforms two-stage, both without KD (10.0 vs. 12.6) and with KD (14.1 vs. 14.8). Since the neck and head jointly handle cross-modal fusion and region-text matching, they form a natural functional unit. Separating them also introduces the need for an independent neck KD strategy, yet distilling multi-scale feature pyramids proves unstable under low-bit settings [50]⁴. These results confirm that the two-stage grouping is the optimal partition strategy.

⁴ Three-stage with neck feature distillation yields AP 13.3, lower than without (AP 14.1).

Table 5: Effect of curriculum stages. 3-stage uses 1/3 data per stage. LVIS miniVal AP is reported.

Curriculum stages	KD	AP
2 (backbone→neck-head)	✗	12.6
	✓	14.8
3 (backbone→neck→head)	✗	10.0
	✓	14.1

Table 6: Effect of quantization granularity and bit-width on YOLO-World-L. Ch-Ch-H = per-channel activations. LVIS miniVal AP is reported.

Granularity	Bits	Method	AP
Ch-T-H	4-5-8	QAT	21.4
		Ours	22.0
Ch-Ch-H	3-3-8	QAT	17.2
		Ours	18.5

5.4 Analysis

Effect of Quantization Granularity. Table 6 reports performance on YOLO-World-L across different quantization granularities and bit-widths. Relaxing the activation bit-width to 5-bit (Ch-T-H 4-5-8) raises QAT AP to 21.4, and CR-QAT surpasses it at 22.0. With per-channel activation granularity (Ch-Ch-H), even the extreme 3-bit setting (3-3-8) becomes feasible, where CR-QAT still outperforms QAT (18.5 vs. 17.2). These results confirm that CR-QAT is consistently robust with respect to granularity and bit-width changes.

Embedding-to-Confidence Relation Transfer. To verify that preserving inter-region relations in the embedding space also benefits the confidence level, we compare the distortion of region-region relational matrices measured in two spaces on 512 LVIS samples (Fig. 3): the embedding space (inter-region semantic similarity) and the confidence space (final classification scores over 1,203 categories). The two quantities exhibit a strong positive correlation ($\rho=0.76$), indicating that distortion of semantic relationships among region embeddings directly propagates to the model’s prediction patterns. Compared to QAT, CR-QAT reduces MAE in both the embedding and confidence spaces, demonstrating that our method effectively preserves the FP32 model’s relational and prediction patterns, which in turn leads to superior detection performance.

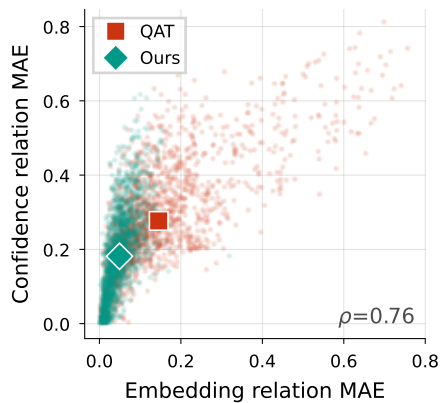


Fig. 3: Correlation between embedding-level and confidence-level inter-region relation distortion relative to FP32. Each point represents an (image, category) group with ≥ 10 anchors. (Large markers) denote the mean over all groups. (ρ) denotes the Spearman correlation.

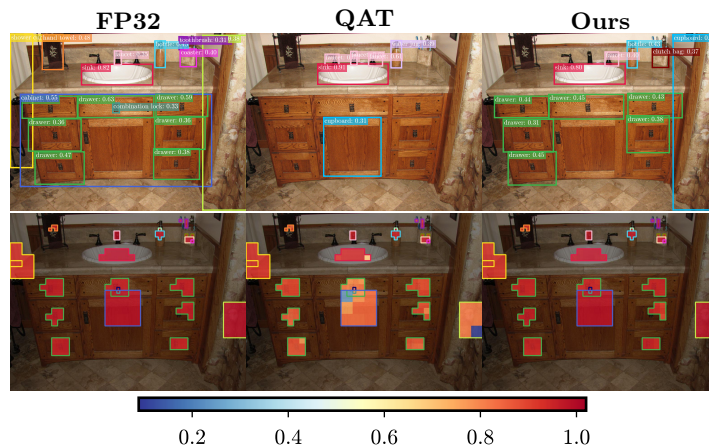


Fig. 4: Qualitative comparison on YOLO-World-L (4-4-8, Ch-T-H). (*Top*) Detection results. (*Bottom*) Inter-region similarity heatmap of average pairwise cosine similarity among same-class anchors. QAT distorts both detection and similarity patterns of FP32, whereas CR-QAT restores them.

Qualitative Analysis. Figure 4 presents a qualitative comparison of zero-shot detection results on an LVIS image. In the detection results (top), QAT shows a significant reduction in the number of detections compared to FP32, missing fine-grained objects, including multiple drawers. CR-QAT substantially recovers these detections. For inter-region similarity (bottom), we visualize the average pairwise cosine similarity of each anchor with other anchors of the same class as a heatmap. We observe that CR-QAT exhibits similarity patterns close to those of FP32, whereas QAT displays notably different patterns, qualitatively supporting the effectiveness of CR-QAT in preserving inter-region relational structures.

6 Conclusion

In this paper, we propose CR-QAT to address the catastrophic degradation of vision-language alignment and inter-region relational structures inherent in extreme low-bit OVOD. To systematically mitigate the accumulation of quantization errors, we formulate CQAT, which guarantees stable optimization via stage-by-stage network partitioning. Concurrently, TRKD explicitly transfers the teacher’s multi-dimensional relational knowledge through the text-anchored pairwise similarity matrices. Extensive evaluations on LVIS and COCO zero-shot benchmarks demonstrate that CR-QAT effectively reconstructs the distorted semantic spaces, consistently outperforming existing QAT baselines under aggressive low-bit settings with relative AP improvements of up to 38.9% and 40.9%, respectively.

References

1. Bengio, Y., Léonard, N., Courville, A.: Estimating or propagating gradients through stochastic neurons for conditional computation. arXiv preprint arXiv:1308.3432 (2013)
2. Bhalgat, Y., Lee, J., Nagel, M., Blankevoort, T., Kwak, N.: LSQ+: Improving low-bit quantization through learnable offsets and better initialization. In: CVPRW. pp. 696–697 (2020)
3. Cao, W., Zhang, Y., Gao, J., Cheng, A., Cheng, K., Cheng, J.: PKD: General distillation framework for object detectors via pearson correlation coefficient. In: NeurIPS. pp. 15394–15406 (2022)
4. Carion, N., Massa, F., Synnaeve, G., Usunier, N., Kirillov, A., Zagoruyko, S.: End-to-end object detection with transformers. In: ECCV. pp. 213–229 (2020)
5. Chen, G., Choi, W., Yu, X., Han, T., Chandraker, M.: Learning efficient object detection models with knowledge distillation. In: NeurIPS. vol. 30 (2017)
6. Chen, P., Liu, J., Zhuang, B., Tan, M., Shen, C.: AQD: Towards accurate quantized object detection. In: CVPR. pp. 104–113 (2021)
7. Cheng, T., Song, L., Ge, Y., Liu, W., Wang, X., Shan, Y.: YOLO-World: Real-time open-vocabulary object detection. In: CVPR. pp. 16901–16911 (2024)
8. Choi, J., Wang, Z., Venkataramani, S., Chuang, P.I.J., Srinivasan, V., Gopalakrishnan, K.: PACT: Parameterized clipping activation for quantized neural networks. arXiv preprint arXiv:1805.06085 (2018)
9. Choukroun, Y., Kravchik, E., Yang, F., Kisilev, P.: Low-bit quantization of neural networks for efficient inference. In: ICCV Workshops. pp. 3009–3018 (2019)
10. Esser, S.K., McKinstry, J.L., Bablani, D., Appuswamy, R., Modha, D.S.: Learned step size quantization. In: ICLR (2020)
11. Feng, C., Zhong, Y., Gao, Y., Scott, M.R., Huang, W.: TOOD: Task-aligned one-stage object detection. In: ICCV. pp. 3490–3499 (2021)
12. Girshick, R., Donahue, J., Darrell, T., Malik, J.: Rich feature hierarchies for accurate object detection and semantic segmentation. In: CVPR. pp. 580–587 (2014)
13. Gu, X., Lin, T., Kuo, W., Cui, Y.: Open-vocabulary object detection via vision and language knowledge distillation. In: ICLR (2022)
14. Gupta, A., Dollár, P., Girshick, R.: LVIS: A dataset for large vocabulary instance segmentation. In: CVPR. pp. 5356–5364 (2019)
15. Gupta, K., Asthana, A.: Reducing the side-effects of oscillations in training of quantized YOLO networks. In: WACV. pp. 2452–2461 (2024)
16. Han, S., Pool, J., Tran, J., Dally, W.: Learning both weights and connections for efficient neural network. In: NeurIPS. vol. 28 (2015)
17. He, Y., Zhang, X., Sun, J.: Channel pruning for accelerating very deep neural networks. In: ICCV. pp. 1389–1397 (2017)
18. Hinton, G., Vinyals, O., Dean, J.: Distilling the knowledge in a neural network. arXiv preprint arXiv:1503.02531 (2015)
19. Hudson, D.A., Manning, C.D.: GQA: A new dataset for real-world visual reasoning and compositional question answering. In: CVPR. pp. 6700–6709 (2019)
20. Jacob, B., Kligys, S., Chen, B., Zhu, M., Tang, M., Howard, A., Adam, H., Kalenichenko, D.: Quantization and training of neural networks for efficient integer-arithmetic-only inference. In: CVPR. pp. 2704–2713 (2018)
21. Jia, C., Yang, Y., Xia, Y., Chen, Y.T., Parekh, Z., Pham, H., Le, Q., Sung, Y.H., Li, Z., Duerig, T.: Scaling up visual and vision-language representation learning with noisy text supervision. In: ICML. pp. 4904–4916 (2021)

22. Jocher, G., Chaurasia, A., Qiu, J.: Ultralytics YOLOv8. <https://github.com/ultralytics/ultralytics> (2023)
23. Kim, J., Bhalgat, Y., Lee, J., Patel, C., Kwak, N.: QKD: Quantization-aware knowledge distillation. arXiv preprint arXiv:1911.12491 (2019)
24. Li, L.H., Zhang, P., Zhang, H., Yang, J., Li, C., Zhong, Y., Wang, L., Yuan, L., Zhang, L., Hwang, J., Chang, K., Gao, J.: Grounded language-image pre-training. In: CVPR. pp. 10955–10965 (2022)
25. Li, R., Wang, Y., Liang, F., Qin, H., Yan, J., Fan, R.: Fully quantized network for object detection. In: CVPR. pp. 2810–2819 (2019)
26. Lin, T.Y., Goyal, P., Girshick, R., He, K., Dollár, P.: Focal loss for dense object detection. In: ICCV. pp. 2999–3007 (2017)
27. Lin, T.Y., Maire, M., Belongie, S., Hays, J., Perona, P., Ramanan, D., Dollár, P., Zitnick, C.L.: Microsoft COCO: Common objects in context. In: ECCV. pp. 740–755 (2014)
28. Liu, S., Zeng, Z., Ren, T., Li, F., Zhang, H., Yang, J., Jiang, Q., Li, C., Yang, J., Su, H., Zhu, J., Zhang, L.: Grounding DINO: Marrying DINO with grounded pre-training for open-set object detection. In: ECCV. pp. 38–55 (2024)
29. Liu, W., Anguelov, D., Erhan, D., Szegedy, C., Reed, S., Fu, C.Y., Berg, A.C.: SSD: Single shot multibox detector. In: ECCV. pp. 21–37 (2016)
30. Liu, Z., Lin, Y., Cao, Y., Hu, H., Wei, Y., Zhang, Z., Lin, S., Guo, B.: Swin transformer: Hierarchical vision transformer using shifted windows. In: ICCV. pp. 10012–10022 (2021)
31. Minderer, M., Gritsenko, A., Stone, A., Neumann, M., Weissenborn, D., Dosovitskiy, A., Mahendran, A., Arnab, A., Dehghani, M., Shen, Z., et al.: Simple open-vocabulary object detection. In: ECCV. pp. 728–755 (2022)
32. Nagel, M., Amjad, R.A., Van Baalen, M., Louizos, C., Blankevoort, T.: Up or down? adaptive rounding for post-training quantization. In: ICML. pp. 7197–7206 (2020)
33. Nagel, M., Baalen, M.v., Blankevoort, T., Welling, M.: Data-free quantization through weight equalization and bias correction. In: ICCV. pp. 1325–1334 (2019)
34. Nagel, M., Fournarakis, M., Bondarenko, Y., Blankevoort, T.: Overcoming oscillations in quantization-aware training. In: ICML. pp. 16318–16330 (2022)
35. Polino, A., Pascanu, R., Alistarh, D.: Model compression via distillation and quantization. In: ICLR (2018)
36. Radford, A., Kim, J.W., Hallacy, C., Ramesh, A., Goh, G., Agarwal, S., Sastry, G., Askell, A., Mishkin, P., Clark, J., et al.: Learning transferable visual models from natural language supervision. In: ICML. pp. 8748–8763 (2021)
37. Redmon, J., Divvala, S., Girshick, R., Farhadi, A.: You only look once: Unified, real-time object detection. In: CVPR. pp. 779–788 (2016)
38. Redmon, J., Farhadi, A.: YOLOv3: An incremental improvement. arXiv preprint arXiv:1804.02767 (2018)
39. Ren, S., He, K., Girshick, R., Sun, J.: Faster R-CNN: Towards real-time object detection with region proposal networks. In: NeurIPS. pp. 91–99 (2015)
40. Shao, S., Li, Z., Zhang, T., Peng, C., Yu, G., Zhang, X., Li, J., Sun, J.: Objects365: A large-scale, high-quality dataset for object detection. In: ICCV. pp. 8430–8439 (2019)
41. Tian, Z., Shen, C., Chen, H., He, T.: FCOS: Fully convolutional one-stage object detection. In: ICCV. pp. 9627–9636 (2019)
42. Wang, C.Y., Bochkovskiy, A., Liao, H.Y.M.: YOLOv7: Trainable bag-of-freebies sets new state-of-the-art for real-time object detectors. In: CVPR. pp. 7464–7475 (2023)

43. Xu, S., Li, Y., Lin, M., Gao, P., Guo, G., Lü, J., Zhang, B.: Q-DETR: An efficient low-bit quantized detection transformer. In: CVPR. pp. 3842–3851 (2023)
44. Zareian, A., Rosa, K.D., Hu, D.H., Chang, S.F.: Open-vocabulary object detection using captions. In: CVPR. pp. 14393–14402 (2021)
45. Zhang, H., Li, F., Liu, S., Zhang, L., Su, H., Zhu, J., Ni, L.M., Shum, H.Y.: DINO: DETR with improved denoising anchor boxes for end-to-end object detection. In: ICLR (2023)
46. Zhang, H., Zhang, P., Hu, X., Chen, Y.C., Li, L., Dai, X., Wang, L., Yuan, L., Hwang, J.N., Gao, J.: GLIPv2: Unifying localization and vision-language understanding. In: NeurIPS. pp. 36067–36080 (2022)
47. Zhang, Y., Dong, Z., Yang, H., Lu, M., Tseng, C.C., Du, Y., Keutzer, K., Du, L., Zhang, S.: QD-BEV: Quantization-aware view-guided distillation for multi-view 3D object detection. In: ICCV. pp. 3825–3835 (2023)
48. Zhong, Y., Yang, J., Zhang, P., Li, C., Codella, N., Li, L.H., Zhou, L., Dai, X., Yuan, L., Li, Y., Gao, J.: RegionCLIP: Region-based language-image pretraining. In: CVPR. pp. 16793–16803 (2022)
49. Zhou, S., Ni, Z., Zhou, X., Wen, H., Wu, Y., Zou, Y.: DoReFa-Net: Training low bitwidth convolutional neural networks with low bitwidth gradients. arXiv preprint arXiv:1606.06160 (2016)
50. Zhu, K., He, Y.Y., Wu, J.: Quantized feature distillation for network quantization. In: AAAI. vol. 37, pp. 11452–11460 (2023)
51. Zhu, X., Su, W., Lu, L., Li, B., Wang, X., Dai, J.: Deformable DETR: Deformable transformers for end-to-end object detection. In: ICLR (2021)
52. Zhuang, B., Liu, L., Tan, M., Shen, C., Reid, I.: Training quantized neural networks with a full-precision auxiliary module. In: CVPR. pp. 1488–1497 (2020)